

Beamline Spectroscopy of Integrated Circuits With Hard X-ray Transition Edge Sensors at the Advanced Photon Source

T. Guruswamy, L. Gades, A. Miceli, U. Patel, O. Quaranta

Abstract—At Argonne National Laboratory, we are developing hard X-ray (2 to 20 keV) Transition Edge Sensor (TES) arrays for beamline science. The significantly improved energy resolution provided by superconducting detectors compared to semiconductor-based energy-dispersive detectors, but with better collection efficiency than wavelength-dispersive instruments, will enable greatly improved X-ray emission and absorption spectroscopic measurements. A prototype instrument with 24 microwave-frequency multiplexed pixels is now in testing at the Advanced Photon Source (APS) 1-BM beamline. Initial measurements show an energy resolution ten times better (150 eV compared to < 15 eV) than the silicon-drift detectors currently available to APS beamline users, and in particular demonstrate the ability to resolve closely-spaced emission lines in samples containing multiple transition metal elements, such as integrated circuits. Comparing fluorescence spectra of integrated circuits measured with our TESs at the beamline to those measured with silicon detectors, we find emission lines and elements largely hidden (e.g. Hf alongside Cu) from a semiconductor-based detector but well resolved by a TES. This directly shows the strengths of TES-based instruments in fluorescence mapping.

Index Terms—superconducting detectors, transition edge sensors, X-ray spectrometers, X-ray fluorescence, integrated circuits

I. INTRODUCTION

SUPERCONDUCTING photon detectors offer an order of magnitude improvement in energy resolution over semiconductor-based detectors. This has enabled them to make a significant impact in a variety of scientific fields, including astronomy, particle physics, and X-ray science [1], [2]. Instruments based on arrays of superconducting Transition Edge Sensors (TESs) are now being deployed at a number of X-ray light sources worldwide [3], [4]. At the Advanced Photon Source (APS), Argonne National Laboratory, we are developing a hard X-ray TES array-based instrument for X-ray

Fluorescence (XRF) and X-ray Absorption (XAS) spectroscopy. Once commissioned, this instrument will be made available for beamline user science.

With their high photon collection efficiency and excellent energy resolution, one potential application for TES-based X-ray spectrometers is high spatial resolution X-ray fluorescence mapping. In this technique, an image is created by scanning the sample with a very focused X-ray beam, measuring X-ray fluorescence spectra at each sampled spatial position to obtain relative elemental abundances. Collecting photons with a high efficiency is important to map quickly, and a high energy resolution is important to correctly identify the fluorescence lines and determine the elemental ratios at each sample point. TESs have an advantage over narrow band, low collection efficiency wavelength-dispersive instruments by covering a wide energy range in a single measurement, and for radiation-sensitive samples which do not allow detector inefficiencies to be compensated for by increasing the incident beam brightness. They also have a large advantage over lower-resolution semiconductor-based energy dispersive instruments for complex samples with mixed 3d, 4d, and 5d transition metal elements with overlapping K and L-shell emission lines. Integrated circuits are an example of samples in this latter category. Besides their semiconductor substrate, integrated circuits consist of complex 3-D geometries of metals and metal compounds. Precisely mapping these features non-destructively requires X-ray wavelengths due to their size [5], [6]. Such a map might be needed for independent verification of correct manufacture, reverse engineering, or failure analysis [7].

The applications of a TES XRF mapping instrument at a synchrotron are similar to those of TES imaging spectrometers in electron microscopes [2] and particle-induced X-ray emission (PIXE) instruments [8]. A synchrotron-based instrument can additionally make use of the monochromatic, very high photon flux X-ray beam tunable over a wide energy range (3 keV to 100 keV at the APS), nano-scale control of the spatial and temporal distributions of incident X-rays, and exotic (e.g. high pressure or temperature) sample environments. This allows for measurements of very dilute or weakly scattering samples, as well as simultaneous measurements with other techniques such as ptychography, Energy-dispersive Diffraction (EDD), Compton imaging, Extended X-ray Absorption Fine Structure (EXAFS), and Resonant Inelastic X-ray Scattering (RIXS). Though our current APS instrument with its prototype TES arrays is not intended for imaging applications, as a demonstration of the concept we have used it to collect

Manuscript received DDD; revised DDD; accepted DDD. This research was supported by Laboratory Directed Research and Development (LDRD) funding from Argonne National Laboratory, and the Accelerator and Detector R&D program in Basic Energy Sciences' Scientific User Facilities (SUF) Division at the Department of Energy; used resources of the Advanced Photon Source and Center for Nanoscale Materials, U.S. Department of Energy Office of Science User Facilities operated for the DOE Office of Science by Argonne National Laboratory under Contract No. DE-AC02-06CH11357, and the Pritzker Nanofabrication Facility of the Institute for Molecular Engineering at the University of Chicago, which receives support from Soft and Hybrid Nanotechnology Experimental (SHyNE) Resource (NSF ECCS-2025633), a node of the National Science Foundation's National Nanotechnology Coordinated Infrastructure. (Corresponding author: T. Guruswamy.)

The authors are with the X-ray Science Division, Argonne National Laboratory, Lemont, IL 60439 USA (e-mail: tguruswamy@anl.gov).

fluorescence spectra from three different integrated circuit chips at the APS beamline, and made a direct comparison against spectra of the same samples collected with a silicon drift detector. This is both a characterization of our system and a simple demonstration of what future purpose-built TES XRF mapping instruments [9] might be able to achieve.

II. INSTRUMENT DESIGN

Our standard TES pixel design features 120 μm -square MoCu bilayers connected to “sidecar”-style absorbers [10], [11]. Normal metal (Cu) features including banks and bars atop the bilayer act to reduce noise [12]. The thin SiN membrane supporting each pixel thermally isolates it from the substrate; the thermal conductance is further reduced by a series of perforations around its perimeter. Here the absorber consists of a 700 μm -square of 1 μm thick sputtered Au, which is sufficient to stop 14% of 20 keV photons. Devices with an additional 10 μm electroplated Bi on the absorbers are now being fabricated; this will raise the stopping power at 20 keV to 63%. As Bi has a heat capacity C at least an order of magnitude smaller than Au, we do not expect the energy resolution ($\propto C^{1/2}$) to be significantly degraded [13]. We have previously shown adding Bi to similar TES arrays results in no measurable change in energy resolution, and the larger grain size of electroplated Bi is preferred over evaporated Bi to avoid energy trapping at grain boundaries [14].

We have fabricated and tested multiple 24-pixel arrays of this design at Argonne National Laboratory. Detailed characterization measurements are consistent with those previously reported [10]; our typical bilayers have a superconducting transition temperature near 87.5 mK, and a normal state resistance near 8 m Ω . The thermal conductance G and heat capacity C are largely controlled by the absorber dimensions; we find $G \sim 500 \text{ pW} \cdot \text{K}^{-1}$ and $C \sim 4 \text{ pJ} \cdot \text{K}^{-1}$. Si collimators with etched 400 μm -square apertures and 10 μm thick electroplated Au are mounted over the TES array to ensure photons are incident only on the absorbers. The collimators include lithographically-defined step features at their corners, which fix both their horizontal position and vertical separation relative to the TES array. Fig. 1(b) is a photograph of two 24-pixel arrays mounted with collimators. The collimator edge has cutouts to allow wire bonds and Cu spring clamps access to the TES array underneath. Al wire bonds connect to the readout circuitry, and Au bonds to the perimeter of the TES array and collimator aid thermalization.

The TES array readout is multiplexed using microwave frequency multiplexing [15]. Each pixel is coupled to an RF SQUID and superconducting microwave resonator (bandwidth 300 kHz) on a nearby multiplexing chip fabricated by the Quantum Sensors Group at NIST. Appropriate shunt resistors (300 m Ω) and fixed inductors (100 nH) are also included in the TES bias circuit. The TESs are voltage biased in series, and the SQUID responses are linearized using flux ramp modulation [16], so in total only one coaxial pair and two DC pairs of wires are needed to read out an entire array. The generation, measurement, and demodulation of the appropriate tones for each resonator is done using a ROACH2-based FPGA

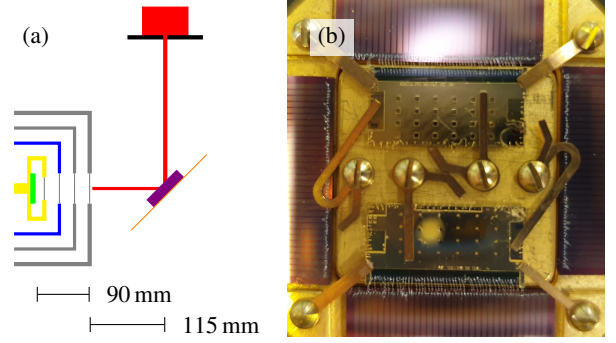


Figure 1. (a) Schematic of experimental setup, top-down view (not to scale). Monochromatic X-ray beam from synchrotron (red) is reduced in size by upstream slits (black). Sample (violet) is mounted on Kapton tape in a standard scattering geometry, at a 45° orientation to both beam and detector. Scattered X-rays pass through windows in the cryostat outer vacuum jacket and inner radiation shields, mu-metal magnetic shielding, and detector box (yellow), illuminating the TES array (green). (b) Photograph of two 24-pixel TES arrays, with collimators, mounted in detector box. The X-rays illuminate approximately the entire center square. Measurements reported here are from the top device with 400 μm square collimator apertures; bottom collimator has 150 μm square apertures. See [10, Fig. 1] for images of the TES array itself.

system [17]. In its current configuration, a single ROACH2-based readout rack of ours provides continuous digitized readout of up to 128 TES pixels at a 62.5 kHz sampling rate. Raw data from each pixel are then processed into pulse records using software-based triggering, and saved. Offline optimal filtering with gain, arrival time and time drift correction is used to extract the best estimate of pulse energy from each saved record [18].

III. MEASUREMENT METHODS

A 24-pixel TES die was mounted in our combined He₃ adsorption/ADR cryostat, which has been installed at the APS 1-BM-C beamline experimental station since November 2019. This cryostat has a “snout” which allows for the TES sensor array to be oriented towards the sample, in the horizontal plane of the beam. It maintains the array at its operating temperature of 60 mK for up to 80 hours, allowing for efficient use of X-ray beam time. X-rays are allowed through the cryostat vacuum jacket by a circular Beryllium window, then through the internal radiation shields, mu-metal passive magnetic shielding, and detector housing by windows of Al foil as shown in Fig. 1(a). The outermost window 90 mm from the sensors with radius 20 mm limits the instrument field of view.

Initial beamline characterization of the TES pixels, by detecting fluorescence from simple metal foils illuminated by a monochromatic X-ray beam at an energy of at least 15 keV, demonstrated a typical energy resolution of 12 eV to 15 eV. This was determined by fits to the K α emission line complexes of various 3d metals (Mn, Fe, Cu), accounting for their intrinsic line width. The best energy resolutions were obtained when the incident photon rates were kept below 3 Hz per pixel and the average measured photon energy kept below 12 keV. Increasing either the photon energy or photon rate significantly beyond this worsened the energy resolution, despite the pixels remaining far from saturation; we are investigating whether this degradation

is related to thermal or electrical cross-talk between pixels, or pulse pile-up on the same pixel.

Three integrated circuit chips, unpackaged bare dies, were selected for the proof-of-concept XRF measurements. These samples were all of different process technologies, manufactured at commercial foundries. We chose a 250 nm CMOS chip, a 350 nm CMOS chip, and a 130 nm SiGe BiCMOS chip, all approximately 10 mm by 20 mm. The exact metal stacks used are proprietary formulations, so the elemental compositions of these chips were not known to us beforehand. The chips were secured to Kapton film, and held with the front face of the chip exposed in the standard 45° scattering geometry shown in Fig. 1(a). The 22.5 keV monochromatic X-ray beam illuminated a 5 mm by 3 mm area near the center of each chip. This beam spot size was chosen to ensure a low (less than 2 Hz per TES pixel) incident count rate at the detector. Spectra were collected with the TES array for at least 8 hours, and then with a single-pixel Vortex silicon-drift detector for a similar length of time (at a much higher count rate, above 1 kHz).

The Vortex silicon-drift detector was separately calibrated using fluorescence from the same Mn, Fe, and Cu metal foils. The TES pixels were calibrated directly from the integrated circuit spectra after the prominent peaks in the measured data were identified. For each pixel and each measurement, a power-law calibration curve was fitted to the identified peaks in the optimal-filtered pulse height histogram. We found the response of each pixel was linear over the energy range 4 keV to 20 keV. In this series of measurements, 15 of the 24 TES pixels in the array both measured sufficient counts and calibrated correctly. The inoperative pixels are primarily attributed to wiring defects or post-fabrication damage. The calibrated data from each working pixel were co-added and binned to produce an energy histogram for each sample, each containing 10^5 to 10^6 total counts.

IV. RESULTS AND DISCUSSION

The measured spectra are presented in Fig. 2 to 4. Counts from the TES pixels and the Vortex have been normalized by the total counts collected for easier comparison. As expected, the measurements expose the presence of several transition metals. Emission lines from W and Cu dominate the 250 nm CMOS and 350 nm CMOS spectra (Fig. 2 and 3). Most peaks are well resolved by the TES, except for Au $L_{\alpha 1}$ (9713 eV) which is visible only as a high-energy shoulder of the W $L_{\beta 1}$ (9672 eV) peak. A very small number of background counts are introduced to the TES-measured spectra by fluorescence from the Au collimator and absorber, and stray fluorescence from Pb elsewhere in the beamline hutch. These contributions were verified by comparison to the XRF spectra of a bare Si wafer. Otherwise, there are very few background counts and little evidence for low-energy tails or non-Gaussian peak shapes, resulting in easily interpretable spectra. W and Cu are known to be present in integrated circuit interconnects and vias [19]. The 250 nm CMOS and 350 nm CMOS spectra are only distinguished by a small difference in the ratios of Cu to W; the 250 nm chip has 1.5 times more Cu than the 350 nm chip, measured relative to W. This is consistent for both the TES and Vortex-measured spectra.

Fig. 4 shows the measured fluorescence spectra from the 130 nm SiGe BiCMOS chip. Although both the TES-measured and Vortex-measured spectra show clear differences from the CMOS chips, in particular a significant increase in Cu, only in the TES-measured spectra is it straightforward to identify the additional presence of Co, Ta and Hf. In particular, the primary lines from these elements – Hf L_{α} (7899 eV) and Ta L_{α} (8146 eV) – cannot be separated from the Cu K_{α} peak (8048 eV) by the Vortex. Quantitative analysis of the TES-measured spectra can therefore be performed much more simply and with much more statistical confidence. In SiGe processes, Co silicides are often used to form the connections between semiconductor elements and the metallic interconnects [20], TaN is a common resistor material, and Hf may be a component of high- k dielectrics for capacitors. We also know that as process nodes have reduced in feature size, Cu has become preferred over other metals for interconnects due to its lower resistivity [21].

The long collection time of the TES-measured spectrum can be easily shortened without impacting the total counts collected by scaling up the number of pixels, at least to our readout capabilities (128 pixels). Further increases may be realized by modifying the pixel design to reduce the pulse decay time, in particular by increasing the thermal conductance. This has only a very weak effect on the energy resolution.

V. CONCLUSIONS

The spectra collected demonstrate that a hard X-ray TES-based energy dispersive detector at a synchrotron can provide high-resolution, broadband spectroscopy to efficiently characterize samples with complex combinations of transition metals, like integrated circuits. The current energy resolution of our pixels, 12 eV to 15 eV, is already sufficient to demonstrate large advantages over a Vortex silicon-drift detector (energy resolution at best 130 eV). Weak emission lines within one hundred eV in energy of a prominent peak are completely invisible to the Vortex, but are able to be identified by the TES array. Although we cannot confirm the exact elemental abundances in these samples due to their proprietary nature, we can claim success in distinguishing different process nodes. While our current instrument does not have imaging capabilities, future instruments will do so [9]; and these, possibly in combination with highly focused light sources like those in development as part of the ongoing APS Upgrade (APS-U), will be able to perform detailed fluorescence mapping to non-destructively analyze integrated circuits at high spatial resolutions. As integrated circuit design and fabrication processes continue to become more complex and separated from their end users, this capability to map their internal structures will become increasingly essential, and we believe TES-based X-ray instruments will play a major part.

ACKNOWLEDGMENT

The authors would like to thank M. Wojcik for assistance with the beamline setup, and the members of the Quantum Sensors Group, NIST (Boulder, CO USA), for their advice on TES design as well as providing and helping implement the μ -mux readout system.

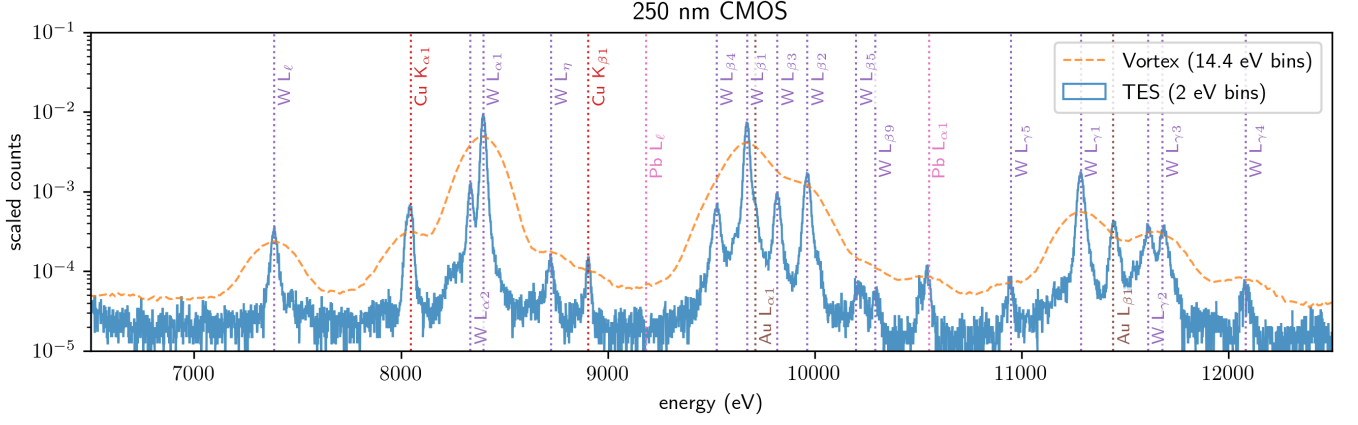


Figure 2. Fluorescence spectra of a 250 nm CMOS integrated circuit chip, measured with a TES sensor (blue solid line) and a Vortex silicon-drift detector (orange dashed line). Emission lines from W and Cu are visible in both measurements; prominent peaks are labeled with their corresponding element and line name.

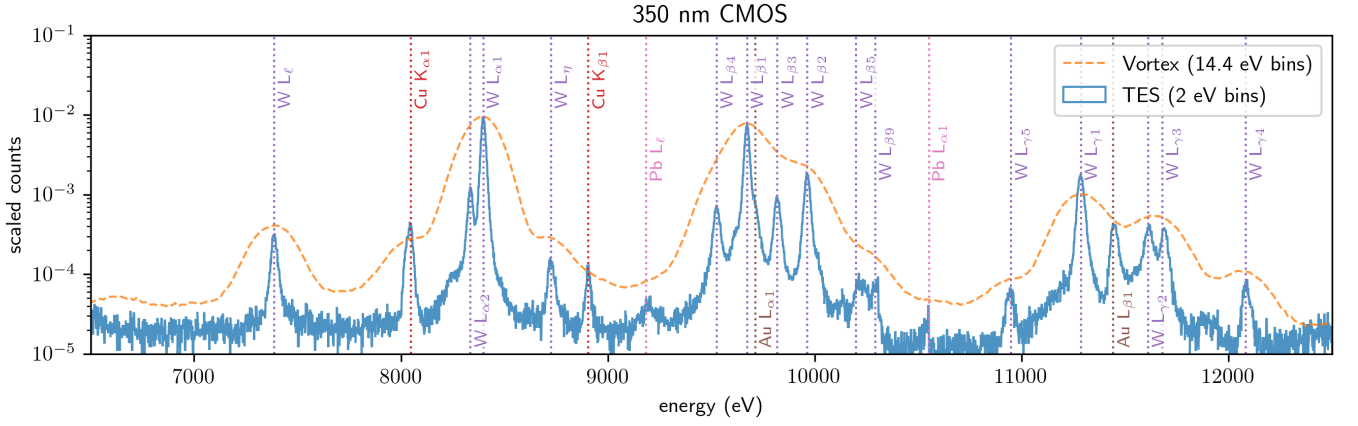


Figure 3. Fluorescence spectra of a 350 nm CMOS integrated circuit chip, measured with a TES sensor (blue solid line) and a Vortex silicon-drift detector (orange dashed line). Prominent peaks are labeled with their corresponding element and line name.

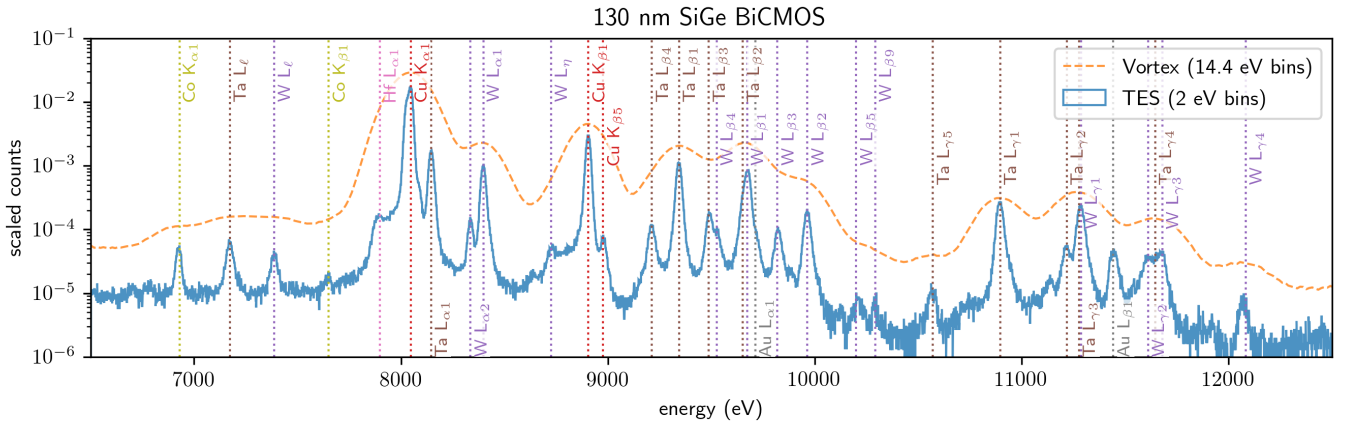


Figure 4. Fluorescence spectra of a 130 nm SiGe BiCMOS integrated circuit chip, measured with a TES sensor (blue solid line) and a Vortex silicon-drift detector (orange dashed line). Relative to the other chips, emission lines from Co, Ta, and Hf are also present, but are clearly resolved only in the TES-measured spectrum.

REFERENCES

- [1] K. Irwin and G. Hilton, "Transition-edge sensors," in *Cryogenic Particle Detection*. Springer, Berlin, Heidelberg, 2005, pp. 63–150. doi: 10.1007/10933596_3
- [2] J. N. Ullom and D. A. Bennett, "Review of superconducting transition-edge sensors for x-ray and gamma-ray spectroscopy," *Supercond. Sci. Technol.*, vol. 28, no. 8, p. 084003, Aug. 2015. doi: 10.1088/0953-2048/28/8/084003
- [3] W. B. Doriese *et al.*, "A practical superconducting-microcalorimeter X-ray spectrometer for beamline and laboratory science," *Rev. Sci. Instrum.*, vol. 88, no. 5, p. 053108, May 2017. doi: 10.1063/1.4983316
- [4] S.-J. Lee *et al.*, "Soft X-ray spectroscopy with transition-edge sensors at Stanford Synchrotron Radiation Lightsource beamline 10-1," *Rev. Sci. Instrum.*, vol. 90, no. 11, p. 113101, Nov. 2019. doi: 10.1063/1.5119155
- [5] Z. H. Levine, A. R. Kalukin, S. P. Frigo, I. McNulty, and M. Kuhn, "Tomographic reconstruction of an integrated circuit interconnect," *Appl. Phys. Lett.*, vol. 74, no. 1, pp. 150–152, Dec. 1998. doi: 10.1063/1.123135
- [6] G. Xu, D. E. Eastman, B. Lai, Z. Cai, I. McNulty, S. Frigo, I. C. Noyan, and C. K. Hu, "Nanometer precision metrology of submicron Cu/SiO₂ interconnects using fluorescence and transmission x-ray microscopy," *J. Appl. Phys.*, vol. 94, no. 9, pp. 6040–6049, Oct. 2003. doi: 10.1063/1.1614430
- [7] K. Mahmood, P. L. Carmona, S. Shahbazzmohamadi, F. Pla, and B. Javidi, "Real-time automated counterfeit integrated circuit detection using x-ray microscopy," *Appl. Opt.*, vol. 54, no. 13, pp. D25–D32, May 2015. doi: 10.1364/AO.54.000D25
- [8] M. R. J. Palosaari *et al.*, "Broadband Ultrahigh-Resolution Spectroscopy of Particle-Induced X Rays: Extending the Limits of Nondestructive Analysis," *Phys. Rev. Applied*, vol. 6, no. 2, p. 024002, Aug. 2016. doi: 10.1103/PhysRevApplied.6.024002
- [9] P. B. Weichman and E. M. Lavelly, "Fluorescent X-ray Scan Image Quality Prediction," *J. Hardw. Syst. Secur.*, vol. 4, no. 1, pp. 13–23, Mar. 2020. doi: 10.1007/s41635-019-00084-8
- [10] T. Guruswamy, L. M. Gades, A. Miceli, U. M. Patel, J. T. Weizerick, and O. Quaranta, "Hard X-ray fluorescence measurements with TESs at the Advanced Photon Source," in *Journal of Physics: Conference Series*, vol. 1559. IOP Publishing, Sep. 2020, Art. no. 012018. doi: 10.1088/1742-6596/1559/1/012018
- [11] U. Patel, R. Divan, L. Gades, T. Guruswamy, D. Yan, O. Quaranta, and A. Miceli, "Development of Transition-Edge Sensor X-ray Microcalorimeter Linear Array for Compton Scattering and Energy Dispersive Diffraction Imaging," *J. Low Temp. Phys.*, vol. 199, no. 1-2, pp. 384–392, Apr. 2020. doi: 10.1007/s10909-019-02267-7
- [12] J. N. Ullom, W. B. Doriese, G. C. Hilton, J. A. Beall, S. Deiker, W. D. Duncan, L. Ferreira, K. D. Irwin, C. D. Reintsema, and L. R. Vale, "Characterization and reduction of unexplained noise in superconducting transition-edge sensors," *Appl. Phys. Lett.*, vol. 84, no. 21, pp. 4206–4208, May 2004. doi: 10.1063/1.1753058
- [13] A.-D. Brown *et al.*, "Absorber Materials for Transition-Edge Sensor X-ray Microcalorimeters," *J. Low Temp. Phys.*, vol. 151, no. 1, pp. 413–417, Apr. 2008. doi: 10.1007/s10909-007-9669-2
- [14] D. Yan *et al.*, "Eliminating the non-Gaussian spectral response of X-ray absorbers for transition-edge sensors," *Appl. Phys. Lett.*, vol. 111, no. 19, p. 192602, Nov. 2017. doi: 10.1063/1.5001198
- [15] J. A. B. Mates *et al.*, "Simultaneous readout of 128 X-ray and gamma-ray transition-edge microcalorimeters using microwave SQUID multiplexing," *Appl. Phys. Lett.*, vol. 111, no. 6, p. 062601, Aug. 2017. doi: 10.1063/1.4986222
- [16] J. A. B. Mates, K. D. Irwin, L. R. Vale, G. C. Hilton, J. Gao, and K. W. Lehnert, "Flux-ramp modulation for SQUID multiplexing," *J. Low Temp. Phys.*, vol. 167, no. 5-6, pp. 707–712, Jun. 2012. doi: 10.1007/s10909-012-0518-6
- [17] J. D. Gard, D. T. Becker, D. A. Bennett, J. W. Fowler, G. C. Hilton, J. A. Mates, C. D. Reintsema, D. R. Schmidt, D. S. Swetz, and J. N. Ullom, "A scalable readout for microwave SQUID multiplexing of transition-edge sensors," *J. Low Temp. Phys.*, vol. 193, no. 3-4, pp. 485–497, Nov. 2018. doi: 10.1007/s10909-018-2012-2
- [18] J. W. Fowler, B. K. Alpert, W. B. Doriese, Y. I. Joe, G. C. O'Neil, J. N. Ullom, and D. S. Swetz, "The practice of pulse processing," *J. Low Temp. Phys.*, vol. 184, no. 1, pp. 374–381, Jul. 2016. doi: 10.1007/s10909-015-1380-0
- [19] Z. H. Levine and B. Ravel, "Identification of materials in integrated circuit interconnects using x-ray absorption near-edge spectroscopy," *J. Appl. Phys.*, vol. 85, no. 1, pp. 558–564, Dec. 1998. doi: 10.1063/1.369489
- [20] J. D. Cressler, *Fabrication of SiGe HBT BiCMOS Technology*. CRC Press, Oct. 2018.
- [21] M. T. Bohr, "Interconnect scaling-the real limiter to high performance ULSI," in *Proceedings of International Electron Devices Meeting*, Dec. 1995, pp. 241–244. doi: 10.1109/IEDM.1995.499187